Nanobiotechnology

Deutsche Ausgabe: DOI: 10.1002/ange.201508339
Internationale Ausgabe: DOI: 10.1002/anie.201508339

Systemically Injectable Enzyme-Loaded Polyion Complex Vesicles as In Vivo Nanoreactors Functioning in Tumors

Yasutaka Anraku, Akihiro Kishimura, Mako Kamiya, Sayaka Tanaka, Takahiro Nomoto, Kazuko Toh, Yu Matsumoto, Shigeto Fukushima, Daiki Sueyoshi, Mitsunobu R. Kano, Yasuteru Urano, Nobuhiro Nishiyama, and Kazunori Kataoka**

Abstract: *The design and construction of nanoreactors are important for biomedical applications of enzymes, but lipid- and polymeric-vesicle-based nanoreactors have some practical limitations. We have succeeded in preparing enzyme-loaded polyion complex vesicles (PICsomes) through a facile protein-loading method. The preservation of enzyme activity was confirmed even after cross-linking of the PICsomes. The cross-linked β-galactosidase-loaded PICsomes (β-gal@PICsomes) selectively accumulated in the tumor tissue of mice. Moreover, a model prodrug, HMDER-βGal, was successfully converted into a highly fluorescent product, HMDER, at the tumor site, even 4 days after administration of the β-gal@PICsomes. Intravital confocal microscopy showed continuous production of HMDER and its distribution throughout the tumor tissues. Thus, enzyme-loaded PICsomes are useful for prodrug activation at the tumor site and could be a versatile platform for enzyme delivery in enzyme prodrug therapy.*

Nanocompartments, which are composed of an inner solution phase and a surrounding shell wall, have attracted much attention for various applications, such as the protection/storage of substances, fabrication of nanoreactors, and delivery of therapeutic materials.[1,2] Nanoreactors are potentially useful not only for chemical synthesis, but also for biomedical purposes.[2–11] In particular, the in vivo use of bio-nanoreactors has generated tremendous research interest with respect to therapeutic and diagnostic applications in various diseases. For the development of nanoreactors, the substrate and product should be exchanged between the inner and outer regions; that is, appropriate permeability of the wall of nanocompartments is required.[11–14] Moreover, the encapsulation of a wide variety of catalytic materials is another essential challenge. Several nanoreactor systems have been developed, but the encapsulation process and permeation of the substrate and products are still big issues in these previous examples.

Most nanocompartments are composed of amphiphilic molecules. Liposomes, polymersomes, and water-in-oil-in-water emulsions have been intensively developed for drug-delivery vehicles.[15–17] However, the preparation of these vehicles usually involves harsh processes, for example, the use of chemicals (organic solvents), sonication, heating, or multiple extrusions. These cumbersome processes often result in the deactivation of the fragile enzymes. Moreover, the permeability of substrates and products is limited owing to the highly hydrophobic walls of the nanocompartments. We previously reported the development of pegylated polyion complex (PIC) vesicles, PICsomes, which can be fabricated simply in an aqueous medium, can directly encapsulate proteins, and have a semipermeable vesicle wall.[18–20] PICsomes enable the uptake of substrates and release of products of enzymatic reactions, and retain enzymes inside their cavity for long durations.[20] Furthermore, cross-linking of the PIC membrane makes PICsomes robust, thus enabling prolonged circulation in the blood and selective tumor accumulation.[21,22] Therefore, enzyme-loaded nanoreactors constructed on the basis of PICsomes are potentially useful for targeting specific tissues in the body. However, an important issue is the preservation of enzymatic activity for a prolonged time period after PICsome delivery into a target tissue, because enzymes may be fragile in harsh in vivo environments. In this study, the activity of enzyme-loaded cross-linked PICsomes was carefully examined under in vivo conditions after systemic intravenous administration. In particular, we demonstrated that β-galactosidase-loaded PICsomes (β-gal@PICsomes) functioned as in vivo nanoreactors only at the target tumor tissue and preserved their enzyme activity even 4 days after systemic administration. Furthermore, with a single dose of β-gal@PICsomes, we

[*] Dr. Y. Anraku, S. Fukushima, D. Sueyoshi, Prof. K. Kataoka
Graduate School of Engineering, The University of Tokyo
7-3-1 Hongo, Bunkyo-ku, Tokyo 113–8656 (Japan)
E-mail: kataoka@bmw.t.u-tokyo.ac.jp
Homepage: http://www.bmw.t.u-tokyo.ac.jp/
Dr. A. Kishimura
Faculty of Engineering, Center for Molecular Systems (CMS)
Kyushu University
744, Moto-oka, Nishi-ku, Fukuoka, 819-0395 (Japan)
E-mail: kishimura@mail.cstm.kyushu-u.ac.jp
Dr. M. Kamiya, Prof. Y. Urano
Graduate School of Medicine, The University of Tokyo
7-3-1 Hongo, Bunkyo-ku, Tokyo 113-0033 (Japan)
Dr. S. Tanaka, Prof. M. R. Kano
Graduate School of Medicine, Dentistry, and Pharmaceutical Science
Okayama University
1-1-1 Tsushima-naka, Kita-ku, Okayama 700–8530 (Japan)
Dr. K. Toh, Dr. Y. Matsumoto, Prof. K. Kataoka
Division of Clinical Biotechnology, Center for Disease Biology and Integrative Medicine, The University of Tokyo
Hongo 7-3-1, Bunkyo-ku, Tokyo 113-0033 (Japan)
Dr. T. Nomoto, Prof. N. Nishiyama
Polymer Chemistry Division, Chemical Resources Laboratory
Tokyo Institute of Technology
4259 Nagatsuta, Midori-ku, Yokohama 226–8503 (Japan)

Supporting information and ORCID(s) from the author(s) for this article are available on the WWW under http://dx.doi.org/10.1002/anie.201508339.

succeeded in in vivo fluorescence imaging of the target tumor and real-time tracking of the enzymatic reaction at the tumor site on the basis of the strong fluorescence of the products.

The encapsulation of enzymes without any chemical modification is desired to preserve enzyme activity. In this regard, PICsomes are beneficial, since they can encapsulate enzymes directly in aqueous media. However, certain enzymes are not electrostatically neutral, but have some charges on their surface, which may disturb PIC formation. Recently, we found a unique response of PICsomes to mechanical stress, whereby PICsomes underwent fragmentation into pairs of single aniomer and catiomer polymer chains, or unit PICs (uPICs), and reassociation took place after the removal of such perturbations.[23] In particular, this reversible association/dissociation is applicable to the loading of enzymes such as β-gal, which is negatively charged at pH 7.4 ($pI \approx 4.6$; molecular weight (MW): 540000), into PICsomes (Figure 1).[20] Also, we demonstrated that β-gal

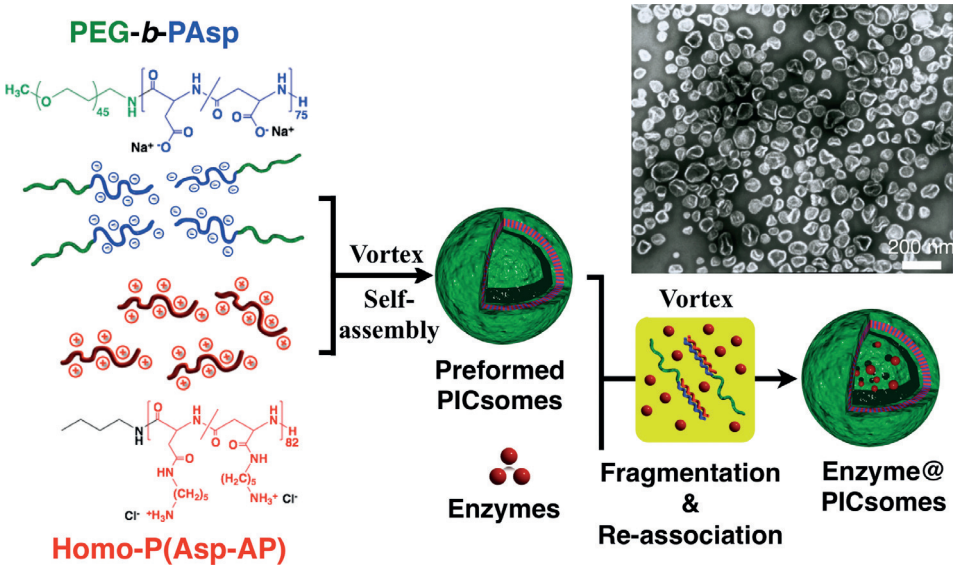

Figure 1. Chemical structures of the constituent polymers of PICsomes, and preparation of enzyme@PICsomes via preformed PICsomes. Top right: TEM image of β-gal@PICsomes (scale bar: 200 nm). PEG = poly(ethylene glycol).

was located in the inner hollow space of PICsomes, as verified by the resistance of β-gal@PICsomes to protease digestion.[20] This result is quite promising for the suppression of nonspecific interactions between charged polymers and proteins. Accordingly, on the basis of the concept of "preformed PICsomes", a different type of enzyme, lysozymes, which have predominantly positive charges on the surface ($pI \approx 11$; MW = 14000), were tested for loading, along with β-gal. When PEG-based block aniomers (PEG-*b*-PAsp), catiomers (Homo-P(Asp-AP)), and β-gal or lysozyme were simply mixed together (see Figure S1 in the Supporting Information), PICsomes with a narrow size distribution and well-controlled size were not obtained.

Preformed PICsomes were used for loading. Specific mechanical stress, that is, vortex mixing for 2 min, was applied to the PICsomes in the presence of β-gal or lysozyme, followed by cross-linking with 1-ethyl-3-(3-dimethylaminopropyl)carbodiimide (EDC; Figure 1a). The formation of spherical particles with diameters of approximately 100 nm and narrow size distributions (see Figure S1) were confirmed by dynamic light scattering (DLS) and transmission electron microscopy (TEM; Figure 1; see also the Supporting Information; β-gal, average diameter: 102 nm, polydispersity index (PDI): 0.056; lysozyme, average diameter: 105 nm, PDI = 0.088). The ζ-potential of both products was negative (−11 mV), and the same as that of the empty PICsomes. The purity of the obtained β-gal@PICsomes was confirmed by size exclusion chromatography (SEC) after purification by ultrafiltration, thus suggesting successful incorporation of the enzymes into the PICsomes (see Figure S2). The encapsulation efficiency was determined to be 0.9% by using a fluorescent-dye-labeled β-galactosidase. This fairly low efficiency is still an issue with the batch encapsulation process applied in this study, and should be improved in future. Loading of the target materials was confirmed by fluorescence correlation spectroscopy (FCS) with Rhodamine Green labeled β-galactosidase (RG-β-gal; see Figure S3).[19,23–25] We compared normalized autocorrelation curves of solutions of RG-β-gal (100 nM) and RG-β-gal@PICsomes and observed a substantially prolonged fluorescence decay time for the RG-β-gal@PICsome sample, which indicates the loading of RG-β-gal into the PICsomes. Similar behavior was observed for lysozyme encapsulation (see Figure S3). The number of RG-β-gal molceules per PICsome was determined to be 2.3 by taking the molecular brightness (count per molecules; CPM) of the RG-β-gal@PICsomes and dividing it by that of free RG-β-gal (see Table S1 in the Supporting Information). Time-dependent FCS analysis revealed that RG-β-gal@PICsomes showed negligible leaking of RG-β-gal through the cross-linked PIC wall (see Figure S4).

The enzyme activity of the cross-linked β-gal@PICsomes was examined by using a substrate of β-galactosidase, hydroxymethyl-*N*,*N*-diethylrhodol-β-galactopyranoside (HMDER-βGal), as an activity probe. HMDER-βGal shows strong absorption and fluorescence after treatment with β-gal, as previously reported.[26] A solution of β-gal@PICsomes (1.1 units) was added to a series of solutions of HMDER-βGal at 37 °C, and absorbance at 525 nm, corresponding to the absorption of produced HMDER, was recorded (Figure 2a). The results showed a time-dependent increase in absorbance, which suggests that HMDER-βGal successfully accessed the

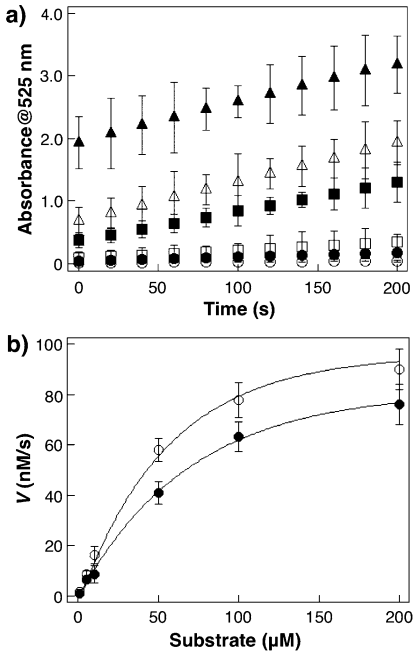

Figure 2. Enzymatic reaction kinetics of β-gal. a) Time course of the increase in absorbance at 525 nm for reaction mixtures with different initial concentrations of HMDER-βGal: 1 (○), 5 (●), 10 (□), 50 (■), 100 (△), and 200 μM (▲). b) Michaelis–Menten plots for β-gal@PICsomes (●) and β-gal (○). *V* is the initial reaction rate of HMDER formation. Error bars on graphs represent mean ± standard deviation (SD).

enzymes across the cross-linked PIC membrane, and was converted into HMDER under the catalysis of the loaded β-gal. We carried out kinetic analysis of HMDER production with a Michaelis–Menten model to estimate the Michaelis constant (K_m) and the maximum reaction rate of HMDER formation (V_{max}; Figure 2b and Table 1). Similar Michaelis–Menten plots were obtained for both the β-gal@PICsomes and β-gal alone, and no significant difference was found for V_{max}, as expected. Notably, the K_m value of the β-gal@PICsomes (82.9 μM) was twice as large as that of β-gal alone (43.3 μM), thus indicating that the affinity of the substrate for β-gal appears to decrease in the presence of the PIC membrane. This difference in affinity might be due to a difference in the accessibility of the enzymes to the substrates or a slight inhibition of product release, possibly owing to the barrier of the PIC membrane. It is considered that the slightly larger molecular weight and/or the greater number of hydroxy groups of HMDER-β-Gal may promote its interaction with the cross-linked PIC network, and accordingly reduce the membrane permeability. Also, the higher hydrophobicity of HMDER may contribute to its prolonged retention in the PICsome cavity, or some charges on the HMDER may facilitate the interaction with the PIC membrane. Since free β-gal was deactivated after treatment with EDC in the absence of PICsomes (data not shown), it appears that the PIC layer protected encapsulated β-gal from the possible attack by EDC during the cross-linking reaction.

Table 1: Kinetic parameters for β-gal@PICsomes and β-gal, as obtained from the Michaelis–Menten plots.

	K_m [μM]	V_{max} [nM/s]
β-gal	43.3 ± 7.2	105.3 ± 6.8
β-gal@PICsomes	82.9 ± 10.2	110.0 ± 8.9

The release of HMDER was confirmed by SEC (see Figure S5). Two peaks were observed in the SEC profile 1 h after the beginning of the reaction, at retention times of the exclusion limit and small compounds (FP detector, $\lambda_{ex}/\lambda_{em}$ = 525/543 nm). In contrast, a single peak was found at the exclusion limit before the addition of the substrate (UV/Vis detector, 220 nm). Therefore, the two peaks found after the enzymatic reaction are assignable to the PICsome-entrapped and released HMDER, respectively. These results suggest that small molecules, such as HMDER, can be released from the inside of the PICsomes, in contrast to large molecules, such as the β-galactosidase.

Next, we evaluated the enzyme delivery of cross-linked β-gal@PICsomes to a target tissue, and their ability to function as in vivo nanoreactors. For this study, murine C26 tumors were subcutaneously inoculated into mice, since the PICsomes with a 100 nm diameter showed selective accumulation in C26 tumor tissues, in accordance with the enhanced permeability and retention (EPR) effect.[21,22] As a proof of concept, an in vivo experiment was designed for the enzymatic reaction in C26 tumor tissue. The in vivo enzyme reaction was visualized by the use of an in vivo imaging system (IVIS, Figure 3a). β-gal@Cy5-PICsomes and β-gal (200 μL, enzyme activity: 10.0 units) were injected intravenously into the tail vein of mice bearing C26 tumors (n = 3). Considering the time for plasma clearance and tumor accumulation of 100 nm PICsomes, a model prodrug, HMDER-βGal, was administered 96 h after the injection of β-gal@Cy5-PICsomes or β-gal. Remarkable fluorescence corresponding to HMDER was found 2 h later only at the tumor site of the mouse treated with β-gal@Cy5-PICsomes (Figure 3a, i). This result indicates that HMDER-βGal was successfully converted into HMDER by the β-gal delivered by the PICsomes, and that the enzymatic activity was maintained even 96 h, or 4 days, after administration. On the other hand, the mouse treated with naked β-gal showed negligible fluorescence from HMDER at the tumor site (Figure 3a, ii). This result is due to the more rapid clearance of bare β-gal from the body, as compared with β-gal@PICsomes. When HMDER-βGal alone was injected into the mouse without any enzyme injection, almost no HMDER fluorescence was detected (Figure 3a, iii). More interestingly, in ex vivo fluorescence imaging, fluorescence of HMDER was detected only from the tumor tissue, whereas negligible fluorescence was found in major organs (liver, lung, spleen, kidney; Figure 3b).

To visualize the entire transplanted tumor, we performed further in vivo imaging by a skin-flap method (Figure 3c).[27,28] For precise determination of the tumor position, C26 tumor tissue expressing green fluorescent protein (GFP-C26) was used. In a mouse injected with β-gal@PICsomes, the region of fluorescence from HMDER coincided with that from GFP,

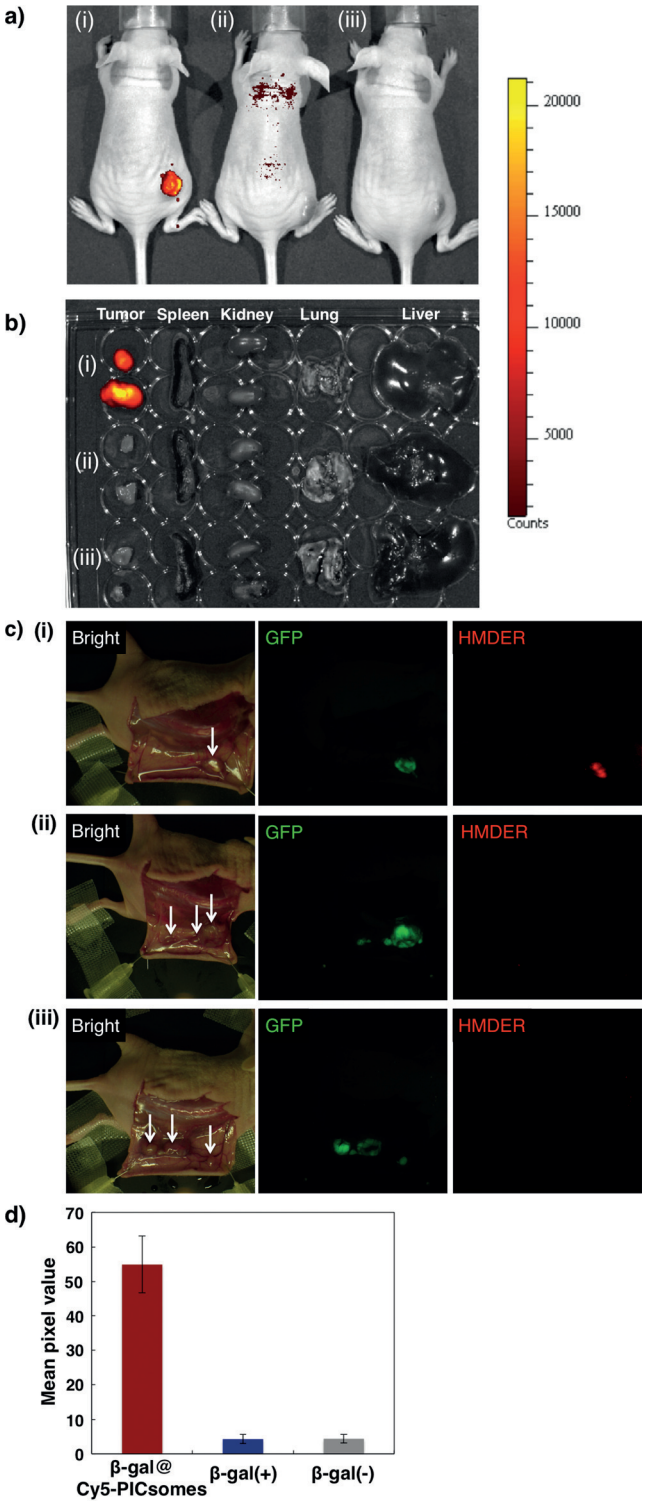

Figure 3. a,b) Macroscopic observation by fluorescence imaging. a) In vivo imaging of C26 tumor mouse, and b) ex vivo imaging of the excised tumor and organs. Filter set: $\lambda_{ex}/\lambda_{em}$ = 500/560 nm. c) In vivo bright-field and fluorescence imaging of GFP-C26 tumors (skin-flap method). Filter sets: $\lambda_{ex}/\lambda_{em}$ = 470/510 nm for GFP, $\lambda_{ex}/\lambda_{em}$ = 540/572 nm for HMDER. White arrows on the bright-field images indicate the position of tumors. d) Quantitative analysis of HMDER distribution in the GFP-C26 tumors (mean ± SD).

and there was no spreading of HMDER beyond the tumor region, thus revealing high tumor selectivity (Figure 3c, i). No HMDER fluorescence was detected in a mouse injected with free β-gal or a control mouse (Figure 3c, ii and iii). The acquired image data were analyzed quantitatively for the average intensity of the HMDER fluorescence by ImageJ software (Figure 3d). The result also showed that significantly greater amounts of HMDER were produced in the tumor by β-gal@Cy5-PICsomes than by free β-gal and the control.

A further histological study was carried out to clarify the extravasation and penetration of β-gal@Cy5-PICsomes and the resulting HMDER in the C26 tumor. Figure 4a clearly

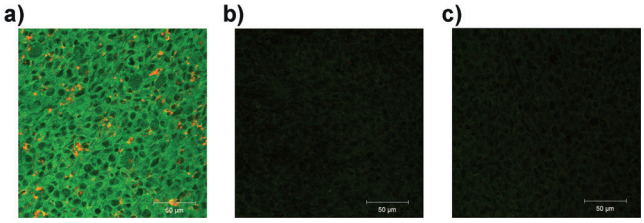

Figure 4. Microdistribution of the PICsomes and HMDER in tumor sections. Fluorescence micrographs of tumor sections prepared from a mouse treated with a) HMDER-βGal and β-gal@Cy5-PICsomes, b) HMDER-βGal and β-gal, and c) HMDER-βGal alone. Green: HMDER; red: Cy5. Scale bars: 50 μm.

shows the distribution of β-gal@Cy5-PICsomes (red) in the C26 tumor tissue. In contrast, the produced HMDER (green) was diffused throughout the cell, except the nucleus, which can be observed as a small dark spot, and was distributed uniformly in the entire tumor tissue. These results are consistent with a previous report describing the ready penetration of HMDER into and diffusion throughout the cell, except the nucleus and Golgi body, owing to high lipid solubility,[26] and our finding that the region of HMDER is localized within the tumor tissue. On the other hand, green fluorescence was not observed in mice treated with bare enzymes or no enzymes (Figure 4b,c).

Acquired image data were quantitatively analyzed for the average intensity of the fluorescence in each image by ImageJ software (see Figure S6). The results also showed that a significant amount of HMDER was produced only when β-gal@Cy5-PICsomes were used and firmly demonstrate that the loading of enzymes into PICsomes enables a dramatic improvement in enzyme disposition, and in the reaction of the enzymes with prodrugs specifically at the tumor site. Although it is not clear from the image shown in Figure 4a whether PICsomes were taken up by cells located in the tumor tissue, β-gal@PICsomes are assumed to function in intracellular as well as extracellular environments, because the substrate, HMDER-βGal, can permeate through the cell membrane,[26] and β-gal can tolerate the acidic environment of intracellular endosomal compartments.[27]

Next, we analyzed the production and distribution of HMDER at the tumor site in a time-resolved manner by intravital real-time confocal microscopy (IVRT-CLSM). This technique enables the spatiotemporal and quantitative anal-

ysis of such behavior as the extravasation and tissue penetration of nanocarriers in a living animal.[28–30] β-gal@Cy5-PICsomes and β-gal (200 μL, enzyme activity: 10.0 units) were injected intravenously into the tail vein of C26-tumor-bearing mice. Subsequently, HMDER-βGal (1 μM, 200 μL) was administered to the mice 96 h after injection of the enzymes. Sequential fluorescence IVRT-CLSM images were collected around the C26 tumor tissues up to 3 h after the injection of HMDER-βGal (Figure 5a–c). Before the injection of HMDER-βGal, fluorescence from the β-gal@Cy5-PICsomes (red spots) was found throughout the tumor tissue, thus indicating explicit tumor accumulation due to the EPR effect (Figure 5a). Upon administration of HMDER-βGal to the mice treated with β-gal@Cy5-PICsomes, green fluorescence corresponding to HMDER was gradually enhanced in the entire tumor, even at positions away from the region of red spots corresponding to β-gal@Cy5-PICsomes. This result indicates that HMDER-βGal was successfully converted into HMDER, which was released from the PICsomes and spread throughout the tumor tissue. On the other hand, free β-gal (Figure 5b) and the control without the injection of β-gal (Figure 5c) revealed no significant enhancement of fluorescence. By normalizing the fluorescence intensities with blank fluorescence in the tumor tissue over time, we obtained time-dependent profiles of the relative fluorescence intensity of HMDER (Figure 5d; blue curve: injection of β-gal@Cy5-PICsomes; red curve: injection of free β-gal). These results also clarify that HMDER production by β-gal@Cy5-PICsomes increased up to about 110 min, which indicates that the enzymatic reaction lasts for at least about 2 h, presumably until the supply of HMDER-βGal from the bloodstream becomes negligible. The fluorescence signal was 11.2 times higher than that of β-gal alone in the tumor tissue at 144 min after injection of the substrate (Figure 5d, blue curve). Thus, β-gal@Cy5-PICsomes maintained appreciable enzyme activity even 4 days after administration, and continued to function evenly after delivery into the tumor tissues for visualization of the entire tumor tissue.

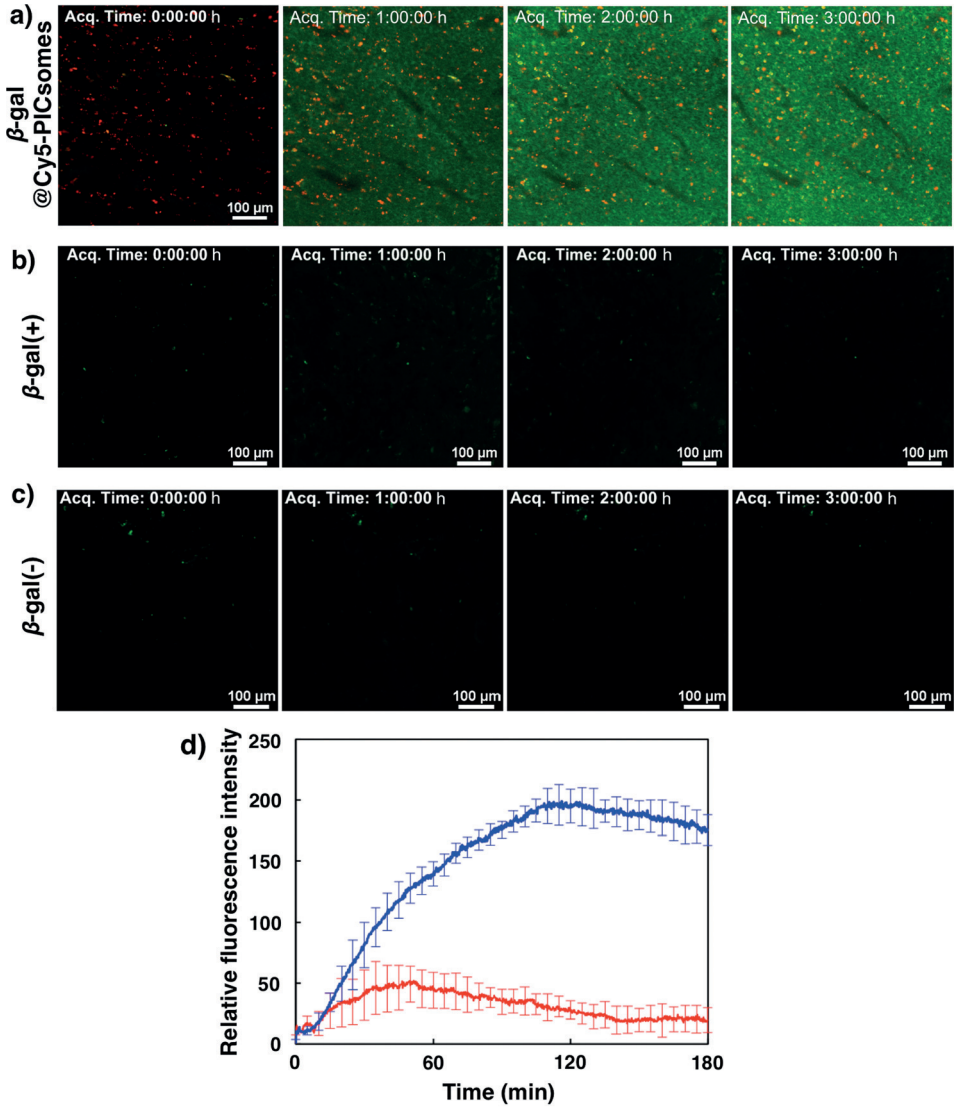

Figure 5. Real-time observation of the enzymatic reaction in C26 tumor tissue by IVRT-CLSM. a–c) Images of C26 tumor tissues at different time points (0, 1, 2, and 3 h after HMDER-βGal injection). β-gal@Cy5-PICsomes (a) and β-gal (b) were injected into the tail vein of C26-tumor-bearing mice. After 96 h, HMDER-βGal was injected into the tail vein of the tumor-bearing mice. c) HMDER-βGal was injected into the tail vein of a C26-tumor-bearing mouse without any injection of β-gal (β-gal(−)). d) Time-dependent change in relative fluorescence intensity in the tumors of mice treated with β-gal@Cy5-PICsomes (blue) and β-gal (red).

In summary, we succeeded in developing enzyme-loaded PICsomes as nanoreactors that function in vivo selectively in tumors. On the basis of our results, PICsomes are excellent carriers for enzymes, and enzyme-loaded PICsomes are promising nanoreactors for activating prodrugs at the target tissue and applicable in enzyme/prodrug therapies (EPT) and enzyme-replacement therapies.[31–34] The following requirements for practical applications can be satisfied by PICsome-based nanoreactors: 1) high bioavailability, or avoidance of rapid renal clearance, 2) less nonspecific accumulation, 3) long-term stability under physiological conditions, 4) long-term enzyme activity, 5) reduction of immunogenicity, and 6) efficient access of

enzymes to prodrugs and effective release of products. PICsomes may provide a general platform for EPT, enzyme-replacement therapy, enzyme-based detoxification, and enzyme-triggered tumor imaging.

Acknowledgements

This research was supported in part by a Grant-in-Aid for Scientific Research (No. 23685037, 25107709, and 26288082 to A.K., and 24700476 to Y.A.) from the Ministry of Education, Culture, Sports, Science, and Technology (MEXT) of Japan, Core Research for Evolutional Science and Technology, and Center of Innovation (COI) Program of the Japan Science and Technology Agency (JST), and by the Japan Society for the Promotion of Science (JSPS) through the "Funding Program for World-Leading Innovative R&D on Science and Technology (FIRST Program)," initiated by the Council for Science and Technology Policy (CSTP). A.K. thanks the Naito Foundation of Science for their financial support. We thank the Research Hub for Advanced Nano Characterization at the University of Tokyo for its valuable support in the TEM measurements.

Keywords: drug delivery · enzymes · in vivo imaging · nanoreactors · vesicles

How to cite: *Angew. Chem. Int. Ed.* **2016**, *55*, 560–565
Angew. Chem. **2016**, *128*, 570–575

[1] J. Cui, P. van Koeverden, M. Müllner, K. Kempe, F. Caruso, *Adv. Colloid Interface Sci.* **2014**, *207*, 14–31.
[2] D. M. Vriezema, M. C. Aragone, J. A. A. W. Elemans, J. J. L. M. Cornelissen, A. E. Rowan, R. J. M. Nolte, *Chem. Rev.* **2005**, *105*, 1445–1489.
[3] P. B. Zetterlund, *Polym. Chem.* **2011**, *2*, 534–549.
[4] Q. Chen, H. Schönherr, G. J. Vancso, *Small* **2009**, *5*, 1436–1445.
[5] A. Ranquin, W. Versées, W. Meier, J. Steyaert, P. van Gelder, *Nano Lett.* **2005**, *5*, 2220–2224.
[6] P. Broz, S. Driamov, J. Ziegler, N. Ben-Haim, S. Marsch, W. Meier, P. Hunziker, *Nano Lett.* **2006**, *6*, 2349–2353.
[7] G. Delaittre, I. C. Reynhout, J. J. L. M. Cornelissen, R. J. M. Nolte, *Chem. Eur. J.* **2009**, *15*, 12600–12603.
[8] S. F. M. van Dongen, M. Nallani, J. J. L. M. Cornelissen, R. J. M. Nolte, J. C. M. van Hest, *Chem. Eur. J.* **2009**, *15*, 1107–1114.
[9] Y.-D. Lee, C.-K. Lim, A. Singh, K. Koh, J. Kim, I. K. Kwon, S. Kim, *ACS Nano* **2012**, *6*, 6759–6766.
[10] Y. Liu, J. Du, M. Yan, M. Y. Lau, J. Hu, H. Han, O. O. Yang, S. Liang, W. Wei, H. Wang, J. Li, X. Zhu, L. Shi, W. Chen, C. Ji, Y. Lu, *Nat. Nanotechnol.* **2013**, *8*, 187–192.
[11] I. Louzao, J. C. M. V. Hest, *Biomacromolecules* **2013**, *14*, 2364–2372.
[12] J. Gaitzsch, D. Appelhans, L. Wang, G. Battaglia, B. Voit, *Angew. Chem. Int. Ed.* **2012**, *51*, 4448–4451; *Angew. Chem.* **2012**, *124*, 4524–4527.
[13] M. Spulber, A. Najer, K. Winkelbach, O. Glaied, M. Waser, U. Pieles, W. Meier, N. Bruns, *J. Am. Chem. Soc.* **2013**, *135*, 9204–9212.
[14] X. Wang, G. Liu, J. Hu, G. Zhang, S. Liu, *Angew. Chem. Int. Ed.* **2014**, *53*, 3138–3142; *Angew. Chem.* **2014**, *126*, 3202–3206.
[15] T. M. Allen, P. M. Cullis, *Adv. Drug Delivery Rev.* **2013**, *65*, 36–48.
[16] P. V. Pawar, S. V. Gohil, J. P. Jain, N. Kumar, *Polym. Chem.* **2013**, *4*, 3160–3176.
[17] M. Ye, S. Kim, K. Park, *J. Controlled Release* **2010**, *146*, 241–260.
[18] A. Koide, A. Kishimura, K. Osada, W.-D. Jang, Y. Yamasaki, K. Kataoka, *J. Am. Chem. Soc.* **2006**, *128*, 5988–5989.
[19] Y. Anraku, A. Kishimura, M. Oba, Y. Yamasaki, K. Kataoka, *J. Am. Chem. Soc.* **2010**, *132*, 1631–1636.
[20] S. Chuanoi, Y. Anraku, M. Hori, A. Kishimura, K. Kataoka, *Biomacromolecules* **2014**, *15*, 2389–2397.
[21] Y. Anraku, A. Kishimura, A. Kobayashi, M. Oba, K. Kataoka, *Chem. Commun.* **2011**, *47*, 6054–6056.
[22] D. Kokuryo, Y. Anraku, A. Kishimura, S. Tanaka, M. R. Kano, J. Kershaw, N. Nishiyama, T. Saga, I. Aoki, K. Kataoka, *J. Controlled Release* **2013**, *169*, 220–227.
[23] Y. Anraku, A. Kishimura, Y. Yamasaki, K. Kataoka, *J. Am. Chem. Soc.* **2013**, *135*, 1423–1429.
[24] R. Rigler, Ü. Mets, J. Widengren, P. Kask, *Eur. Biophys. J.* **1993**, *22*, 169–175.
[25] P. Rigler, W. Meier, *J. Am. Chem. Soc.* **2006**, *128*, 367–373.
[26] M. Kamiya, D. Asanuma, E. Kuranaga, A. Takeishi, M. Sakabe, T. Nagano, Y. Urano, *J. Am. Chem. Soc.* **2011**, *133*, 12960–12963.
[27] J.-P. Tenu, O. M. Viratelle, J. Garnier, J. Yon, *Eur. J. Biochem.* **1971**, *20*, 363–370.
[28] Y. Matsumoto, T. Nomoto, H. Cabral, Y. Matsumoto, S. Watanabe, R. J. Christie, K. Miyata, M. Oba, T. Ogura, Y. Yamasaki, N. Nishiyama, T. Yamasoba, K. Kataoka, *Biomed. Opt. Express* **2010**, *1*, 1209–1216.
[29] H. Cabral, Y. Matsumoto, K. Mizuno, Q. Chen, M. Murakami, M. Kimura, Y. Terada, M. R. Kano, K. Miyazono, M. Uesaka, N. Nishiyama, K. Kataoka, *Nat. Nanotechnol.* **2011**, *6*, 815–823.
[30] H.-J. Kim, M. Oba, F. Pittella, T. Nomoto, H. Cabral, Y. Matsumoto, K. Miyata, N. Nishiyama, K. Kataoka, *J. Drug Targeting* **2012**, *20*, 33–42.
[31] H. A. Campbell, L. T. Mashburn, E. A. Boyse, L. J. Old, *Biochemistry* **1967**, *6*, 721–730.
[32] C. S. Fishburn, *J. Pharm. Sci.* **2008**, *97*, 4167–4183.
[33] J. Rautio, H. Kumpulainen, T. Heimbach, R. Oliyai, D. Oh, T. Järvinen, J. Savolaonen, *Nat. Rev. Drug Discovery* **2008**, *7*, 255–270.
[34] D. Niculescu-Duvaz, G. Negoita-Giras, I. Niculescu-Duvaz, D. Hedley, C. J. Springer in *Prodrugs and Targeted Delivery* (Ed.: J. Rautio), Wiley-VCH, Weinheim, **2011**, pp. 271–344.

Received: September 6, 2015
Revised: November 2, 2015
Published online: December 2, 2015

